ANALYTICAL STUDY ON BEHAVIOR OF A R/C FRAME WITH WALLS AND STRUCTURAL GAPS DUE TO EXCESSIVE EARTHQUAKE MOTION

M.Honaga [1], T. Mukai [2], H. Kinugasa [3], Y. Matsuda [4]

[1] *Graduate Student, Tokyo University of Science, 7115123@gmgmail.com*
[2] *Senior Research Engineer, Building Research Institute, t_mukai@kenken.go.jp*
[3] *Professor, Tokyo University of Science, kinu@rs.noda.tus.ac.jp*
[4] *Assistant professor, Tokyo Univ. of Science, Japan, matsuda_y@rs.noda.tus.ac.jp*

Abstract

Today, mainly for simple modeling, many buildings have structural gaps between frame and walls. Analysis for such buildings and evaluation of their seismic safety are performed with the assumption that structural gaps will not become blocked and the frames around them will not be badly affected. However, if an earthquake motion occurs that is larger than expected in structural design, it is expected that horizontal response deformation will cause structural gaps to become blocked and wall members to contact the frames around them. In this case, seismic evaluation for such buildings must be performed while considering these phenomena; however, no such method has been established yet.

By creating an analytical model that takes contact into account, this study aims to understand the behavior of a whole building when wall members contact the frames around them, and to evaluate seismic safety performance including negative effects when contact is made.

Therefore, a nonlinear-pushover analysis is conducted for a full scale five-story reinforced concrete frame specimen with walls and the gaps that exhibited the above behavior. The validity of modeling the behavior of wall members contacting the frame around them as observed during the experiment is investigated by comparing the analytical results with the test results in terms of the horizontal load–deformation relationship, the sequence in which structural members make contact, and the representative deformation angle of the whole building at the time of contact, by specifying a shear spring constant so that horizontal stiffness increases steeply after a certain level of horizontal displacement is reached. Using the analytical results, parameters such as changes in the stress transferred by the contacting peripheral members are checked, and evaluation the seismic safety performance for a whole building will be done.

Keywords: a full scale reinforced concrete building; rectangle-section wall; contact; structural gap; nonlinear pushover analysis

1. Introduction

This paper proposes a new type of structure [1] that can contribute to secure their continuous availability after earthquakes. It is based on RC (reinforced concrete) structural technology that does not require advanced technologies such as vibration control or seismic base isolation, and can be used with conventional structural design methods. This structural type gives higher strength and rigidity to each layer than regular rigid-joint frames. It works by modifying the columns of the rigid-joint frame with sleeve walls, which reduces the maximum response displacement under seismic conditions. This reduction in seismic response can increase the continuous availability of structures after earthquakes following damage to the non-structural parts of buildings.

Experiments conducted by Fukuyama et al. (2015)[1] evaluated the ability of columns with sleeve walls to provide structural gaps and prevent rectangular-section walls from shearing forces. However, the gaps became blocked during the experiment and the rectangular-section walls contacted the spandrel wall and bore shearing forces as a result. Although there is no need to assume that such contact will occur under the levels of earthquake motion that are assumed during the design phase, such contact could occur with stronger earthquakes. On the other hand, although the experiments of Mukai, Kawagoe et al. (2018) demonstrated a modeling method [2, 3] that properly evaluated the behavior noted above, the behavior of a frame with rectangular-sectioned walls in contact with spandrel walls (as described above) has not been investigated. Accordingly, the purpose of this study was to build an analytical model that considers such contact and predicts its behavior. In addition, this paper investigates the seismic safety of frames comprising this type of contact.

2. Outline of experiments

2.1 Outline of specimens

An outline of the specimen (Fukuyama et al. 2015[1]) analyzed in this paper is given in Fig.1. The specimen was a full-scale, solid, five-story, reinforced concrete frame with two spans in the ridge direction (pressurization in-plate direction) and one span in the span direction (pressurization off-plate direction). In addition, it had a structural gap between the wing walls/spandrel walls or hanging partition walls, and between the spandrel walls and rectangular-section walls, so that the wing wall was utilized as the only structural skeleton. The width of the structural gaps between the wing walls/spandrel walls or between the hanging partition walls was 45 mm, and the gaps between the spandrel walls/rectangular-section walls were 80 mm. In Fig.1, the framing elevations in the ridge and span directions are specified in the upper-left and upper-right areas, and a framing plan of a typical floor is specified in the lower-left area. The mechanical characteristics of the reinforced steel and concrete used are specified in Tables 1 and 2, and a sectional view of the column and beam member is given in Fig.2. Sectional views of a rectangular-section wall and wing wall attached to a column are provided in Fig.3. Each wing wall had reinforcing detail on the same edge. Their projecting length were 700 mm and the wall thickness was 200 mm. Reinforcing bars for the wall edge were 6-D16 bound with enclosed-type reinforcing rods. Vertical reinforcement in the walls comprised doubly-arranged D10@200, bound with width-fixing reinforcements (D10) installed in the orthogonal direction. Horizontal reinforcements in the walls were fixed with 180° hooks and linearly fixed at the column cross-sections.

Spacings between the vertical reinforcements in the walls were doubly-arranged D10@100 in the first floor (to control buckling of the vertical reinforcements) and D10@200 in the other floors. Figure 3 provides a representative sectional view of the first floor. It can be computed that a certain degree of ductility capacity is obtained, as the degree of shear allowance was calculated as 1.26 by calculating the flexural ultimate strength based on Bernoulli-Euler theory, and the ultimate shear strength based on a segmentation cumulative equation for the columns with sleeve walls in the first floor.

Figure 4 specifies the bar arrangement of the slab reinforcement. The slab thickness was 200 mm, with D10@50 used for both top and bottom reinforcements in the ridge direction, D10 and D13 arranged alternately at intervals of 150 mm for the top reinforcement, and D10@150 forming the bottom reinforcement in the span

direction. Slab reinforcements within the effective width of the slabs in the span direction were placed in seven rows, with 18.5 rows in the overall width (for both top and bottom reinforcements).
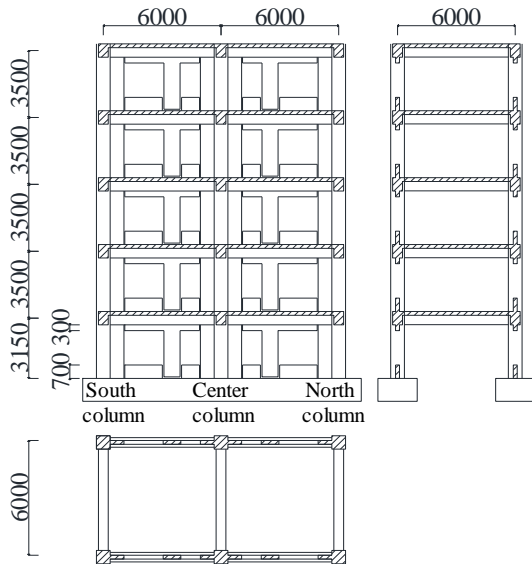

Fig. 1 – Outline of the specimen (unit:[mm])

Table 1 – Material characteristics of the reinforced steel

Reinforced steel		σy (N/mm2)	Es (N/mm2)
D10 (Wall and slab)	SD295	352	182600
D10 (Horizontal reinforcements in the wall)	SD295	372	185100
D13 (Horizontal reinforcements in the column and beam)	SD295	340	182000
D13 (Slab for top reinforcement)	SD295	342	180600
D16	SD295	384	187100
D25 (1F column and beam)	SD345	383	182000
D25 (2~5F column and beam)	SD390	449	181000

σy:Yield strength of reinforced steel, Es:Young's modulus of reinforced steel

Table 2 – Material characteristics of the concrete

Concrete	σB (N/mm2)	Ec (N/mm2)
5F	31.3	24700
4F	33.6	26200
3F	37.7	28500
2F	33.0	26100
1F	34.9	28600

σB:Compressive strength, Ec:Young's modulus of concrete

Fig. 2 – Sectional view of the column and beam (unit:[mm])

Fig. 3 – Sectional views of a rectangular-section wall and wing wall attached to a column (unit:[mm])
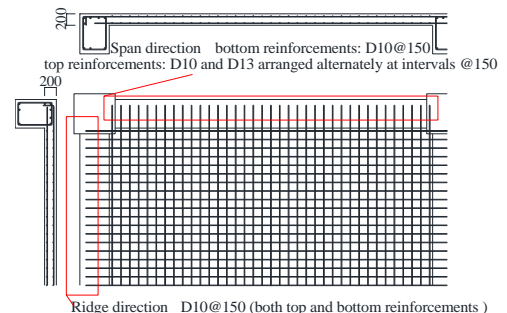

Fig. 4 – The bar arrangement of the slab reinforcement

3

2.2 Loading plan

As shown in Fig.5, pressurization was conducted on 4F and RF with an actuator installed so that the center of the slab thickness was the pressurization core, with a load ratio of 4F:RF = 2:1. Four actuators were installed on both the RF and 4F and the external forces were controlled by the average value of the horizontal displacement of the RF beam core position.

The pressurization cycle comprised positive and negative alternating cyclic loading at the representative deformation angle Rr (horizontal displacement of R layer beam core height/distance from top end of the stub to the R layer beam core height). Loads Rr = 1/1600 rad and 1/800 rad were applied once, Rr = 1/400 rad, 1/200 rad, 1/100 rad, 1/67 rad, and 1/50 rad were applied twice, then Rr = 1/37 rad was applied in the forward direction.

2.3 Measurement plan

The horizontal deformation angle and representative deformation angle Rr of each layer were measured by a horizontal displacement measuring device installed at the beam core position of each layer. The positions of the horizontal displacement measuring devices are specified in Fig.5. Deformation was measured against the main reinforcements of major column/beams, flexural reinforcing bars, and slab reinforcements in the pressurization in-plate direction. Since the deformation of beam bars on the north side was used for examination in this paper, their positions are specified in Figs.6 and 7.

2.4 Experimental results

Figure 8 shows the envelope curve representing the relationship of base shear to representative deformation angle. The maximum strength before the rectangular-section wall contacted the spandrel wall was about 4400
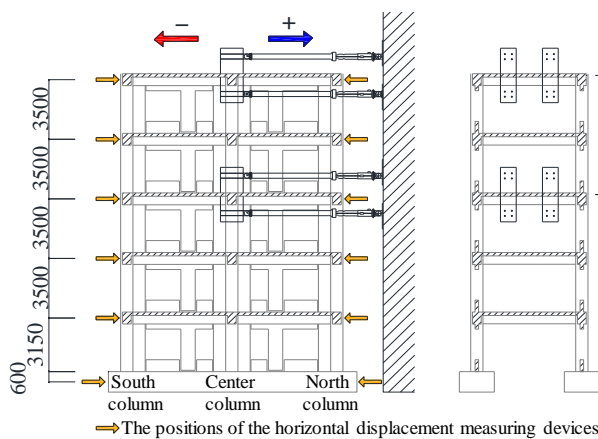

Fig. 5 – Loading device and the positions of the horizontal displacement measuring devices (unit:[mm])
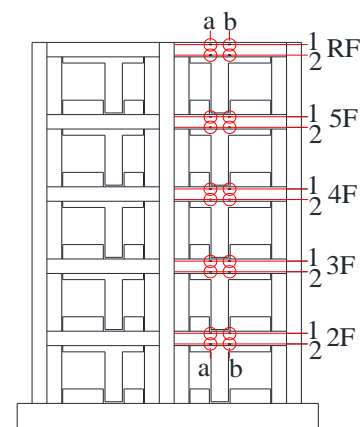

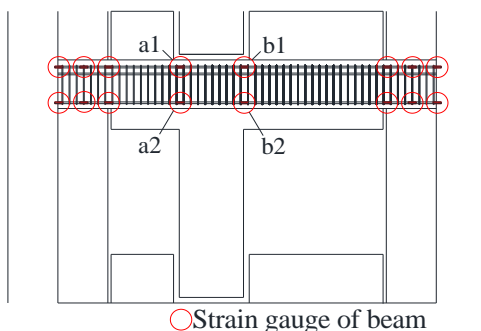Fig. 6 – Strain gauge position of beams near rectangular-section walls (unit:[mm])
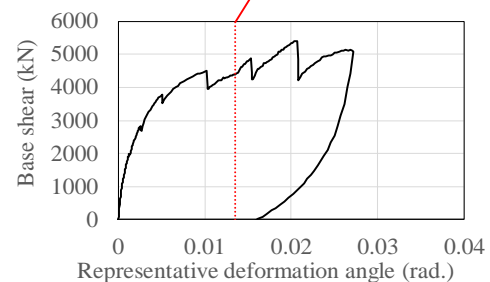

Fig. 7 – Strain gauge position of north beam

Fig. 8 – Relationship of base shear to representative deformation angle

4

kN, demonstrating a maximum strength at the rectangular-section walls at a representative deformation angle of +0.01 rad. In general, strength deterioration was not observed during this period, demonstrating tough behavior. At the point near the representative deformation angle of +0.014 rad, the structural gap in the specimen between the rectangular-section wall and the spandrel wall on the second and third layers was closed and the walls contacted (as shown by the broken line in Fig.8). The rectangular-section wall bore the shearing force by contacting the spandrel wall, and base shear increased at the distortion angle thereafter. In addition, regarding contact between the components described above, since the floor height was 3500 mm while the structural gaps between the rectangular-section and spandrel walls were 80 mm, it was assumed that they would not make contact when the distortion angle reached 0.02 rad (the structural gap was wide enough because 3500 mm × 0.02 = 70 mm). However, contact of the components was observed at a point earlier than this. The cause can be considered to be interlayer deformation, as well as rotation of the rectangular-section wall fitted to the beam that occurred due to deformation of the beam.

3. Outline of the analysis

3.1 Frame modeling

As shown in Fig.9, the frame had a solid frame with each component of the column/beam modeling by line element at the core position of the structure, and nodes were mounted on the joints of each component. The degrees of freedom in movement and rotation were constrained on nodes 1, 2, 3, 19, and 21, as specified in Fig.9.As shown in Fig.9, in accordance with Mukai, Kawagoe et al. (2018)[2], the rigid areas of the columns were on the beam face position, and those of the beams penetrated into the joint sides by only D/4 (where D represents the component depth) from the face position of the columns with the sleeve wall. Dangerous cross-sectional positions occurred on the face positions of the column, beam, and wall.

In addition, the rectangular-section walls were modeled as single columns. In doing so, they were configured so that they would bear the yield strength when displaced enough to contact the spandrel wall. Here, shear springs that caused contact (Figs.9 and 10) were installed. The upper part of the rectangular-section wall was configured as a rigid zone with a length of 650 mm (shown as a bold line in Fig.10). Since the rectangular-section wall contacted the entire spandrel wall in the experiment conducted by Fukuyama et al. (2015)[1], we determined the node height of the lower part of the rectangular-section wall to be the center location of the contacting surface. In addition, to transmit flexural stress to the beam that the rectangular-section wall was attached to, the rectangular-section wall was treated as a stud and the attached beam was divided at the center of the wall depth of the rectangular section of the wall and modeled. Since the divided beam was specified as a single member, a rigid zone was not provided on the beam at the joint of the rectangular-section wall and beam. Although models that have a rigid zone at the joint can be considered adequate, differences between the modelled and experimental values of initial stiffness can arise when contact is made. Furthermore, since there were only small differences in the results of the model without a rigid zone after contact, the study was conducted with a model that did not have a rigid zone on the joint.

A rigid floor was assumed for horizontal pressurization and configured in accordance with the pressurization results by making its center of gravity act as the pressurization point during the experiment. The force strength and control methods were as follows.

・The horizontal force was configured on the center of gravity of the slab at core heights of 4F and RF so the force strength became 4F:RF = 2:1.

・Displacement control was configured so that the horizontal displacement of the rigid floor built on the RF slab core height increased by 0.1 mm per step.

Furthermore, although the external forces used in the experiment alternated between positive and negative, a one-way load was used for this analytical model.

5

The axial force used to calculate the yield strength of the material was configured by estimating the weight of the reinforcing steel and concrete used according to the controlling area of the floor for all nodes. The weight of reinforcing steel and concrete was found by calculating the cubic volume based on the cross-sectional area and floor height of each component. Then, the weight of reinforcing steel was estimated by multiplying the unit volume weight by 76.93 kN/m^3, while the weight of concrete was estimated by multiplying the unit volume weight by 24.5 kN/m^3. The PΔ effect was not considered in this analysis.

3.2   Element modeling

Columns were modeled by placing flexural springs on the edges of the material and placing shear springs and axial springs at the center. The beams were modeled as single-axis springs by placing flexural springs at the edges of the material and shear springs at the center. Flexural and shear springs were regarded as three polygonal line models that took crazing strength and yield strength limits into account. Axial springs were regarded as a two polygonal line model that took the elasticity of the compression side and the yield of reinforcement steel at the tension side into account.

The rectangular-section wall was configured to bear moment and shearing forces. The shear spring used for the consideration of the contact specified in Figs.9 and 10 was configured so that the rigidity would increase suddenly (rigidity was defined as 100 MN/mm) and the rectangular-section wall would bear yield strength once a certain displacement was reached, as shown in Fig.11, since the structural gap between the rectangular-section and spandrel walls was 80 mm. Since this deformation dominated before a large enough stress that could destroy the part that was contacted (because the rectangular-section wall was equipped with a hinge), a simple model that transmits stress through a shear spring with a hard inclination was used in this paper.

○ Shear springs that cause contact
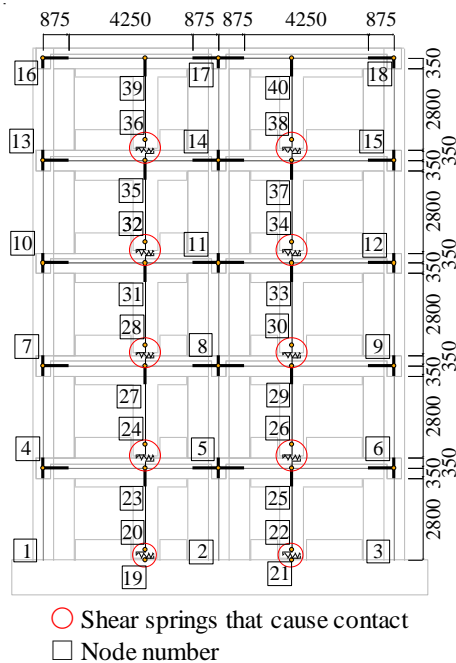□ Node number

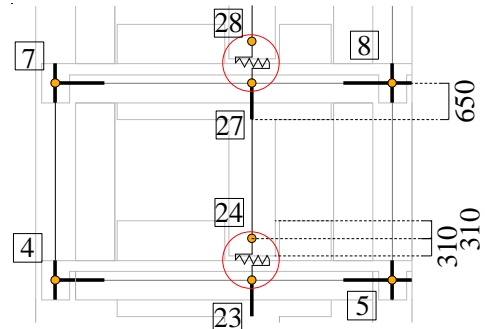Fig. 9 – Frame model considering rectangular-section walls (unit:[mm])

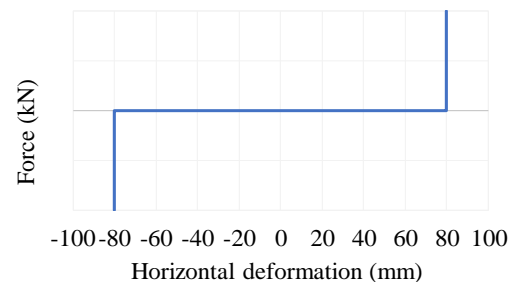Fig. 10 – Details of frame model considering rectangular-section walls

Fig. 11 – Shear spring that cause contact

Regarding the flexural and shear springs of the columns, beam, and rectangular-section walls, the initial stiffness of the flexural spring was calculated by Formula (1), while that of the shear spring was calculated by Formula (2) according to a previous study[4]. In accordance with study[5], Formula (3) was used to calculate the rate of rigidity decrease in the flexural springs used for the columns and beams, while Formula (4) was used for the rectangular-section wall. Formula (5) was used to calculate the rate of rigidity decrease in the shear spring used for the columns and beams in accordance with study[6], while Formula (6) was used for the

6

rectangular-section wall in accordance with study[5]. The flexural and cracking strengths of the columns, beams, and rectangular-section walls were calculated by Formula (7) in accordance with study[5]. Also based on study[5], the shear and crazing strengths were calculated with Formula (8) for the columns and with Formula (9) for the columns for beams. In addition, Formula (10) was used for the shear and crazing strength of the rectangular-section walls. In accordance with document[7], the ultimate flexural strength was calculated with Formula (11) as a reset total solution. Ultimate shear strength was calculated with Formula (12) in accordance with document[5]. Since the rectangular-section walls of the specimen used in this paper hung down to the beams, the yield strength was calculated based only on the strength of the concrete and reinforcing steel, as for the beams, with shaft force of 0. In addition, although the effective width of the slab was determined as 1 m in the study conducted by Mukai, Kawagoe, et al. (2018)[2,3], to get close to the experiment value, the lengths were modified in each floor by assuming the point where the slab reinforcement yielded to be the effective width. Since the maximum yield strength before contact was observed at the point around the representative deformation angle of +0.01 rad, the yielding state of the slab reinforcement at this point can be described by Fig.12.
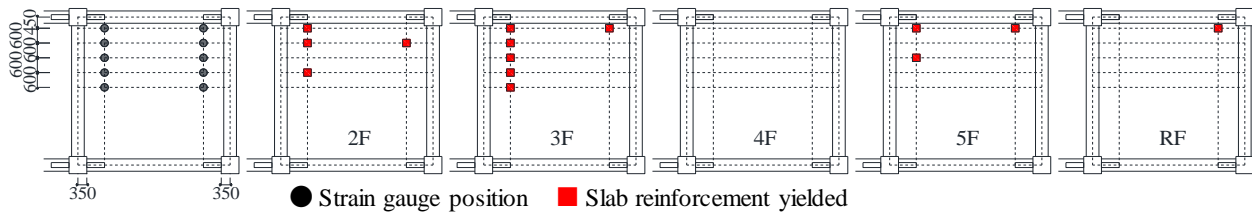

Fig. 12 – Yielding state of the slab reinforcement (representative deformation angle of +0.01 rad.)

Further, it was considered that the strength of the beam changes, since the shearing force borne by the rectangular-section walls acts as a shaft force against the beam when the rectangular-section walls are contacted. However, when the shearing force of the rectangular-section wall calculated during analysis was entered into Formula (11), the change in yield strength was only about 7% compared with models without shaft force. Therefore, fluctuation in the shaft force was not considered in this model.

$$K_f = 6E_cI/L \tag{1}$$

$$K_s = GA/\kappa L \tag{2}$$

$$\alpha_y \begin{cases} (0.043 + 1.64np_t + 0.043\left(\frac{a}{D}\right) + 0.33\eta_0)\left(\frac{d}{D}\right)^2 \\ (-0.0836 + 0.159\left(\frac{a}{D}\right) + 0.169\eta_0)\left(\frac{d}{D}\right)^2 \end{cases}$$

$$2.0 < \text{upper formula if (a/D), } 2.0 \geq \text{lower formula if (a/D)} \tag{3}$$

$$\alpha_y = {}_wM_y C_n /EI_w\varepsilon_y \tag{4}$$

Here, ${}_wM_y$ = yield moment of rectangular section wall [N・mm], C_n = the distance from the elastic neutral axis when the second vertical reinforcement edge from the tension edge is at the yield point to the center of gravity of the vertical reinforcement on the tension side [mm], E = Young's modulus of concrete [N/mm²], I_w = cross-sectional secondary moment [mm⁴], and ε_y = yield strain of vertical reinforcement.

$$\alpha = \left(\frac{Q_{un}}{\gamma_u}\right) / \left(\frac{Q_c}{\gamma_c}\right) \tag{5}$$

7

$$\beta_u = \frac{0.46 p_w \sigma_y}{F_c} + 0.14 \tag{6}$$

$$M_c = (0.56\sqrt{\sigma_B} + \sigma_0)Z_e \quad [\text{N} \cdot \text{mm}] \tag{7}$$

$$Q_c = \left(1 + \frac{\sigma_0}{150}\right)\left(\frac{0.085 K_c (F_c + 500)}{\frac{M}{Qd} + 1.7}\right)\text{bj} \quad [\text{kg}] \tag{8}$$

$$Q_c = \left(\frac{0.085 K_c (F_c + 500)}{\frac{M}{Qd} + 1.7}\right)\text{bj} \quad [\text{kg}] \tag{9}$$

$$V_c = \tau_{scr} t_w l_w / x_w \quad [\text{N}] \tag{10}$$

Here, τ_{scr} represents the shear crazing force of concrete [N/mm²], the tensile strength of concrete is $\sigma_t (= 0.33\sqrt{\sigma_b}$, where σ_b represents the compressive strength of concrete), t_w = the rectangular-section wall thickness [mm], $l_w = 0.9 \times$ inside length of the rectangular-section wall [mm], and x_w = the section modulus, which is the rectangular section multiplied by 1.5.

$$M_u = A_{st}\sigma_{st}d - A_{sc}\sigma_{sc}d_c - \frac{\sigma_{av}b(\beta_1 x_n)^2}{2} + \text{Ng} \quad [\text{N} \cdot \text{mm}] \tag{11}$$

$$Q_u = \left\{\frac{0.068 p_{te}^{0.23}(F_c + 18)}{\sqrt{\frac{M}{QD} + 0.12}} + 0.85\sqrt{\sigma_{wh} p_{wh}} + 0.1\sigma_0\right\} t_e j \quad [\text{kN}] \tag{12}$$

4.   Comparison of analytical and experimental results

4.1   Evaluation of the load-deformation relationship

Figure 13 describes the base shear-representative deformation angle relationships obtained through experiment and theoretical analysis. It shows that the load-deformation relationship is mostly reproducible by letting the shear spring representing the contact bear horizontal force after contacting the rectangular-section wall. The analysis shows that the base shear starts to increase in around a representative deformation angle of 0.013 rad. In addition, Fig.13 shows that the rate of increase in base shear is not constant, which is because the rectangular-section walls are making contact at different times. Analysis shows that the base shear increases suddenly when the rectangular-section walls on 2F and 3F contact for the first time. The rectangular-section wall produces flexural yielding near Point A in Fig.13 and the rigidity is reduced again. After this, the rectangular-section walls on 1F, 4F, and 5F begin to make contact near Point B in Fig.13 and the base shear increases by shearing force. Finally, the base shear stops increasing near Point C in Fig.13, when all rectangular-section walls become flexural-yielding. It is thought that the reason why the yield strength becomes constant is because the degree of shear allowance (ultimate shear strength/ultimate shear strength during flexural) in the rectangular-section walls in this specimen is > 2. Therefore, the walls do not collapse, showing that the specimen has high strength.

4.2   Evaluation of the starting point of contact between the rectangular-section and spandrel walls

This section analyzes the contact starting point through the horizontal displacement of nodes and verifies it by comparison with the experimental data. Figure 14 describes the horizontal displacement of nodes for each representative deformation angle between 2F and 3F. The point where the rate of increase in the horizontal displacement of nodes 24 and 26 (refer to Fig.9) changes under the influence of the shear spring used to consider the contact was regarded as the contact starting point. Figure 14 shows that the rectangular-section

8

wall on the north side contacted the spandrel wall slightly before south side rectangular-section wall. A similar tendency was confirmed among other nodes as well.
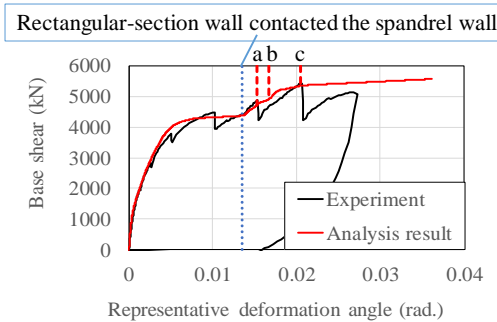

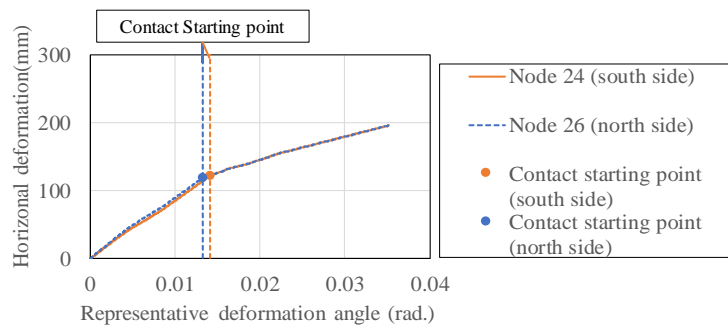Fig. 13 – Relationship of base shear to representative deformation angle

Fig. 14 – Horizontal displacement of nodes for representative deformation angle (2~3F)

The contact starting point in the experiment was estimated by distortion of the beam in the vicinity of the rectangular-section wall. Since beam bar strain gauges were only attached to the rectangular-section walls on the north side in the experiment, the contact starting point on the north side was assumed. The positions of the strain gauges are shown in Figs.6 and 7. In these figures, the upper-left beam of each floor is denoted as a1, the lower-left beam is a2, the upper-right beam is b1, and lower-right beam is b2. As shown in Fig.15, which describes the moments before and after contact, the moment of the beams changes after contact with the rectangular-section walls. Among the strain gauges in the vicinity of the rectangular-section walls, those at b1 and b2 change rapidly. The representative deformation angle at this point was defined as the contact starting point for the experimental values. Figure 15 describes the moments of the rectangular-section wall on the north side of 2F and its peripheral members. The values for beams b1 and b2 on 3F are described in Fig.16 and are representative of the strains on beam bars in the vicinity of the rectangular-section walls. Further, Fig.16 shows the relationship between strain and representative deformation angle within the range Rr = −0.01–0.015 rad. It was confirmed that at locations b1 and b2, a rapid change in strain began at a representative deformation angle of approximately 0.014 rad. The strains of the beams in the other floors were also assumed according to the method above.
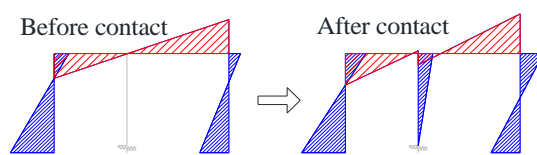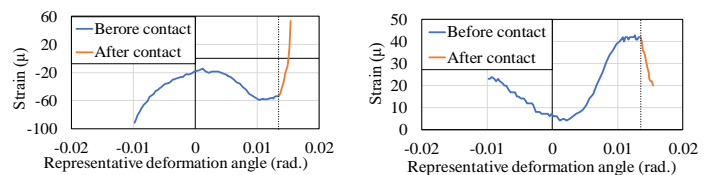

Fig. 15 – Moments before and after contact

Fig. 16 – Strain on beam bars (Left:b1, right:b2)

The contact starting points determined by the method above are compiled in Table 3 so that the experimental and theoretical values can be compared. Since only the contact starting point of the rectangular-section wall on the north side was calculated experimentally, comparison is made with that wall. In addition, contact starting points plotted on the load-deformation angle relationships are shown in Fig.17. In both the experimental and theoretical data, the order of occurrence of contact starting points is 2F and 3F, followed by 1F and 4F, then 5F, which demonstrates that the evaluation was accurate. In addition, we confirmed that the representative deformation angles at the contact starting points were within 0.013–0.020 rad, which is a reasonable range.

Table 3 – Comparison of representative deformation angles at which contact started

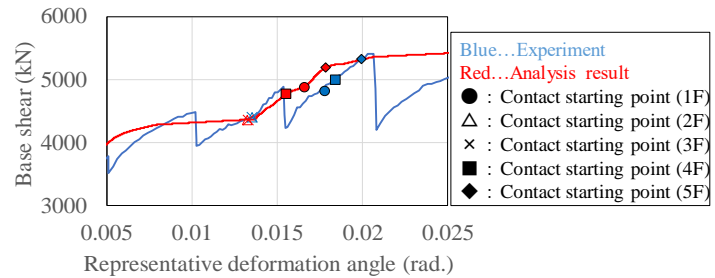| Floor	Experiment (rad.)	Analysis result (rad.)
5F	0.020	0.017
4F	0.018	0.015
3F	0.014	0.013
2F	0.014	0.013
1F	0.018	0.016

Fig. 17 – Comparison of contact starting point

5. Investigation on seismic safety of frames after contact with rectangular-section walls

Flexural yielding occurred on the column bases and terminal members of the beams on 1F in the specimen. Based on a determination that the beams bear the shearing force of the rectangular-section walls, which endangers the beams, we focused on the degree of shear allowance (ultimate shear strength of beams/shearing force of beams) to investigate the safety of the beams used in this study. Regarding calculation methods, we used data such as the theoretical inflection point ratio to re-calculate the ultimate shear strength. The shearing force borne by the beams is the sum of the shearing forces occurring when the beams have a flexural yield and that borne by the rectangular-section walls. A value that accounts for the whole width of the slab as effective width was calculated when estimating the flexural ultimate strength. In addition, calculations were carried out with an assumption that the beams bear a shaft force due to contact with the rectangular-section walls. The ultimate flexural strength and ultimate shear strength were re-calculated by taking the shaft force into account, and calculations were carried out for two cases: 1) when the beams bore a compressive axial force and 2) when the beams bore a tensile axial force. The results are shown in Table 4.

Table 4 – Degree of shear allowance (beam)

		Effective width of the slab (1m)		Effective width of the slab (whole width)	
		Beam (2~4F)	Beam (5F・6F)	Beam (2~4F)	Beam (5F・6F)
Degree of shear allowance（ultimate shear strength of beam /shearing force of beam）	Before contact	2.05	2.48	1.59	1.80
	After contact	1.51	1.72	1.25	1.36
	Compressive axial force consideration	1.46	1.67	1.21	1.32
	Tensile axial force consideration	1.57	1.79	1.28	1.40

Table 4 shows that the degree of shear allowance decreased after contact compared to that before contact, with the lowest value being 1.21. It can be confirmed from this that the possibility of shear fracture increases when there is contact between members of the framework. It will be necessary to investigate the seismic safety of the frame with consideration of earthquakes that are stronger than the expected level, which could cause contact between members of the framework.

Since it can also be assumed that the possibility of shear fracture increases for the columns, we investigated the columns in the first floor, whose column bases had flexural yield. Regarding calculation methods, we used data from the theoretical analysis to re-calculate the ultimate shear strength, as with the beams. We also used theoretical estimates for the shearing force of the columns. In addition, since the shearing force of the columns can change according to the shearing force of the beams, calculations were carried out for each calculation pattern of the beams. The results are shown in Table 5.

It can be confirmed that the degree of shear allowance decreased, as with the beams. Specifically, the lowest value among the center columns in the first floor was 1.13, indicating that a sufficient degree of shear allowance was not ensured.

10

Table 5 – Degree of shear allowance (1F column)

		South column (1F)	Center column (1F)	North column (1F)
Degree of shear allowance （ultimate shear strength of column /shearing force of column）	Before contact	1.76	1.51	2.32
	Beam:Effective width of the slab (1m)	1.47	1.30	2.08
	Beam:effective width of the slab (whole width)	1.29	1.15	1.93
	Beam:axial force consideration (effective width of the slab (1m))	1.45	1.29	2.08
	Beam:axial force consideration (effective width of the slab (whole width))	1.27	1.13	1.93

5.   Conclusions

We conducted a static nonlinear-pushover analysis of the specimen of Fukuyama et al. (2015)[1] with consideration of the behavior occurring when rectangular-section walls contact a spandrel wall, and gained the knowledge described below.

・We were able to experimentally evaluate load-deformation relationships and the sequence in which structural members make contact in a specimen comprising rectangular-section walls and spandrel walls. Shear springs were used where the horizontal stiffness increased rapidly after the point where a specified horizontal displacement was reached. In addition, by making comparisons with experimental values, we confirmed that the representative deformation angle at the contact starting point estimated by theoretical analysis was within a reasonable range.

・It will be necessary to secure slit widths at the design phase to prevent contact between framework members, which can occur when structural gaps are closed during a major earthquake. It is possible to estimate the necessary slit width by applying the model presented in this study.

・It is confirmed that the degree of shear allowance for column and beam members decreases when an unexpectedly strong earthquake occurs, as members of the framework contact each other. From this, it is shown that it is necessary to secure sufficient degrees of shear allowance for columns and beams when considering unusually strong earthquakes.

References

[1] H. Fukuyama, T. Mukai, S. Tajiri, M. Teshigawara, T. Kabeyasawa, H. Suwada, M. Tani and K. Kusunoki (2015): Static Loading Test on A Full Scale Five Story Reinforced Concrete Building utilizing Wing Walls for Damage Reduction, Summaries of Technical Papers of Annual Meeting, Architectural Institute of Japan, Structures-IV, pp.571-572,

[2] T. Mukai, Y. Kawagoe, H. Kinugasa, S. Kono, M. Maeda, M. Tani, H. Watanabe, M. Sakashita (2018): Non-linear Pushover Analysis for Full Scale Five Story Reinforced Concrete Resilient Buildings Utilizing Walls Part1; Outline of Experimental Test and Analysis Method, Summaries of Technical Papers of Annual Meeting, Architectural Institute of Japan, Structures-IV, pp.539-540

[3] Y. Kawagoe, T. Mukai, H. Kinugasa, S. Kono, M. Maeda, M. Tani, H. Watanabe, M. Sakashita (2018): Non-linear Pushover Analysis for Full Scale Five Story Reinforced Concrete Resilient Buildings Utilizing Walls Part2; Comparison of Analysis Results with Experimental Results, Summaries of Technical Papers of Annual Meeting, Architectural Institute of Japan, Structures-IV, pp.541-542

[4] Architectural Institute of japan (2010): AIJ Standard for Structural Calculation for Reinforced Concrete Structures.

[5] National Institute for Land and Infrastructure Management (NILIM), and Building Research Institute (BRI) (2015): Commentary on Structural Regulations in the Building Standard Law of Japan.

[6] H. Umemura (1982): Dynamic Seismic Design Method for Reinforced Concrete Buildings-subsequence (for Middle Building)

[7] Architectural Institute of japan (1997):Design Guidelines for Earthquake Resistant Reinforced Concrete Buildings Basad on Inelastic Displacement Concept (Draft)